21 MAY 1980 FLARE REVIEW

CORNELIS DE JAGER and ZDENĚK ŠVESTKA
Laboratory for Space Research, Utrecht, The Netherlands

Abstract. A review is given of observations and theories relevant to the solar flare of 21 May, 1980, 20 : 50 UT, the best studied flare on record. For more than 30 hr before the flare there was filament activation and plasma heating to above 10 MK. A flare precursor was present ≥ 6 min before the flare onset. The flare started with filament activation (20 : 50 UT), followed by thick-target heating of two footpoints and subsequent ablation and convective evaporation involving energies of 1 to 2 × 10^{31} erg. Coronal explosions occurred at 20 : 57 UT (possibly associated with a type-II burst) and at 21 : 04 UT (associated with an Hα spray?). Post-flare loops were first seen at 20 : 57 UT, and their upward motion is interpreted as a manifestation of successive field-line reconnections. A type-IV radio burst which later changed into a type-I noise storm was related to a giant coronal arch located just below the radio noise storm region. Some implications and difficulties these observations present to current flare theories are mentioned.

1. Introduction

We have selected the major solar flare of 21 May, 1980 for a review, because it was one of the best observed, and best analyzed flares in the whole history of solar research. Its observations on board the Solar Maximum Mission (SMM) spacecraft led to the first study of images of hard X-ray brightenings at footpoints of loops during the impulsive phase (Hoyng *et al.*, 1981) and to the discovery of giant post-flare coronal arches following two-ribbon flares (Švestka *et al.*, 1982a). Antonucci *et al.* (1985) found high-velocity upward motions during the impulsive phase which yield information about the early phase of chromospheric evaporation, and Lemmens and De Jager (1985) found related lateral motions pointing to a chromospheric explosion. During the growth of post-flare loops, Švestka an Poletto (1985) gave a direct evidence for a late release of energy high in the corona which might represent hard X-ray images of the reconnection of field lines. The mass ejection associated with this flare was imaged both by the NRL–Solwind coronagraph on board the P78–1 spacecraft and by the Helios A zodiacal-light photometer (McCabe *et al.*, 1985). Several other papers have analyzed the flare observations and contain attemps to interpret them.

In addition to these observations of the flare itself, we also have good data about the active region in which the flare occurred, because coordinated observations of the region were made for several days as a part of the Flare Build-up Study Program (Harvey, 1983; Schadee *et al.*, 1983). We are thus in possession of an extraordinary set of data on pre-flare variations, the flare build-up, flare onset, impulsive phase, decay phase with post-flare loops, the associated mass ejection, and the post-flare corona. We have tried to summarize these various aspects of this flare event in the following review.

2. Pre-Flare Variations in the Active Region

The major flare (importance 2B/X1) started at 20 : 50 UT on 21 May, 1980 (Hoyng *et al.*, 1981) in Hale region 16850 at 13 S 15 W. The SMM spacecraft pointed at this

Solar Physics **100** (1985) 435–463. 0038–0938/85.15.

active region (with a few short gaps) from 16 UT on 17 May. Schadee *et al.* (1983, further abbreviated as SDJS) analyzed the observations made by the Hard X-Ray Imaging Spectrometer (HXIS) from 12 : 50 UT on 19 May and detected an almost permanent X-ray emission along the filament channel of the active region.

This emission was extremely weak, about 10^{-4} times the 3.5–5.5 keV X-ray flux from an average flare event (cf. SDJS Figure 2 and Table I) so that only long integrations (for 20 min or more) revealed statistically significant X-ray images. The activations along the filament channel lasted apparently long enough, or repeated themselves so often, that most integrations yielded distinct images (cf. SDJS Figure 2). However, in spite of the low countrate, the temperature in these phenomena was found to be close to 11 million degrees, without any involvement of flares or detectable flare-like brightenings (cf. SDJS Table IV).

This high temperature was determined from the (5.5–8.0 keV)/(3.5–5.5 keV) flux ratio under the assumption of a Maxwellian distribution of velocities (thermal plasma, cf. Mewe *et al.*, 1985). Thus it may either represent a real temperature in heated loops embedding the filament or, as Mandelstam and his co-workers (private communication) believe, it may be a fictitious 'temperature' of a non-thermal plasma produced by intermittent, but very frequent accelerations along the filament channel. They base their suggestion on the fact that in some other, possibly analogous, events the ion temperature, deduced from linewidths of X-ray lines, was substantially lower.

As from 14 UT on 20 May this semi-permanent weak X-ray emission along the filament channel began to appear close to the site of the most intense enhancement later seen in the onset phase of the flare (A in Figure 1; cf. SDJS Figure 4). The emission

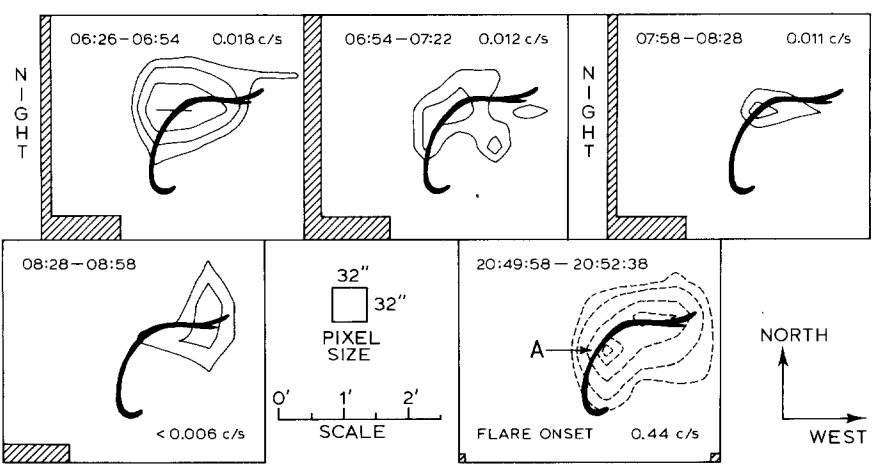

Fig. 1. Last HXIS images on 21 May, 1980 of the long-lived X-ray brightening which coincided in position with the brightest patch (A) of the later coming flare (cf. SDJS, Figure 2) and subsequent shift of the emission to the western end of the filament. Energy range 3.5–5.5 keV in HXIS coarse field of view. The eastern border of the FOV is hatched and the filament is indicated. Data at the top of each frame: UT beginning and end of count integration; mean countrate in the pixel with maximum count. The last frame (with dashed contours) shows the onset of the flare. (After Schadee *et al.*, 1983.)

stayed in this position until ~07 UT on 21 May (see the last images of this period in Figure 1; note that 'close to' means 'within the spatial resolution of 32 arc sec'). It is of interest that at 18 UT on 20 May the zodiacal-light photometer aboard Helios A began to record a weak mass ejection at a distance above 20 solar radii from the Sun. It became most pronounced at 6 UT on 21 May and decayed thereafter until the mass ejection from the major flare succeeded it in about the same position (cf. Figure 2, flare ejection

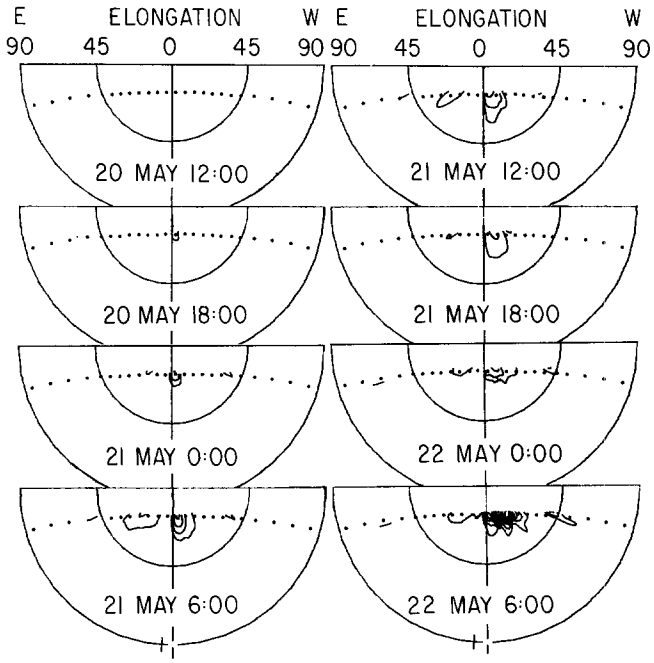

Fig. 2. Helios A photometer images of excess electron density along the line-of-sight in contour steps of 3×10^{14} cm^{-2}. The photometer reading nearest to the Sun is at 16° S from the ecliptic plane; see paper by Jackson in this issue for more information about the plots. (Courtesy of B. Jackson, UCSD, La Jolla.)

appears at 22 May 0:00 and 6:00 UT; see paper by Jackson in this issue for an explanation of the plottings). Thus, from the viewing position of Helios A (30° west from the Sun–Earth line) there was a weak mass-flow into interplanetary space at the position angle of AR 16850 for more than one day prior to the major flare, without any obvious source other than the long-lived brightenings along the filament channel detected close to the position of the later flare by SDJS. This observation tends to support the interpretation by Mandestam's group that the weak X-ray enhancements are images of intermittent acceleration processes along the filament channel.

Also Hα images of the filament showed remarkable changes for at least a day before the flare (Harvey, 1983), though the flare activity was very low (only four Hα subflares were reported during two days preceding the major flare). According to Gaizauskas (in

Harvey, 1983) the main filament changes were seen near its west end, but parts of the filament showed vertical motions which could be interpreted as rotational motions of the filament along its own axis. The western-end activity might have been provoked by the rapidly moving magnetic flux in this area: a nearby spot moved with a mean velocity of 130 m s^{-1} on 20 May and 260 m s^{-1} on 21 May during the five last hours preceding the major flare. Large electric currents flowing along the filament might be the cause of the vertical motions (Harvey, 1983) and of the intermittent instabilities seen in X-rays by HXIS.

3. Flare Build-up and Onset

As Figure 1 shows, X-ray emission at the site of the main brightening of the major flare (site A) ceased to exist between 6 and 8 UT on 21 May and it did not reappear until $\sim 19:20$ UT in the evening (SDJS, Section 3.1.4.). Within the coarse resolution of 32 arc sec its position was then quite identical with the later brightening in the flare. This brightening stayed slightly enhanced (0.014 counts s^{-1}) till 19:53 UT (onset of SAA extending into the SMM night), and reappeared in the same position at 20:44 UT (SMM sunrise) with 0.18 counts s^{-1}, slowly brightening. Faster enhacement (which can be considered to be the flare onset) started at 20:50 UT (imaged in Figure 1) and reached flare intensity at 20:55 UT. Thus one may tentatively assume that a pre-flare X-ray brightening appeared in the active region 90 min before the flare onset, and that with certainty an X-ray precursor was present at $\leq 20:44$ UT, i.e., ≥ 6 min before the flare onset. For a comparison: in another (smaller) flare of 30 April, 1980, with the much better resolution of 8 arc sec in the HXIS fine field of view, De Jager *et al.* (1983) observed a flare precursor exactly at the flare site for ~ 30 minutes prior to the flare.

According to Gaizauskas (in Harvey, 1983), strong downward motions appeared at the west end of the filament about 2 hr before the flare. At the same time, a kink developed in the middle of the filament, very close to the main site of the brightening in the flare, and these changes may have been associated with the pre-flare X-ray enhancement mentioned above. Rust (in Hoyng *et al.*, 1981) suggested that the kink was due to the emergence of new flux exactly below it, manifested by the appearance of a new tiny spot just beneath that position. However, Harvey's (1983) analysis of magnetograms suggests that this spot did not form by emergence but by the compression of existing flux at the surface. This compression was ultimately caused by newly erupting flux, evidenced by the magnetograms, but this flux was located to the west of the spot and the kink. The net flux at a location directly beneath the activated filament actually decreased. Nevertheless, as Gaizauskas (1985) suggests, these changes may have destroyed the equilibrium between the filament and its surroundings, so that emerging flux could have been indirectly the source of the filament disruption and associated flare emission at the site of the kink.

According to Harvey (1983) these magnetic field changes were first detected about 80 min prior to the flare and they increased steadily in strength. This has striking

similarity with the HXIS observations mentioned before: an X-ray enhancement at the position of the brightest flare patch first appeared 90 min prior to the flare and its intensity was continuously growing.

Both Harvey (1983) and Gaizauskas (1985) believe that the described flare build-up and flare onset are consistent with the model of filament eruption of Kuperus and Van Tend (1981). However, according to McCabe *et al.* (1985) the filament did never rise and erupt (cf. Section 8). As the flare developed at the kink, a set of bright Hα loops formed across the neutral line and along it towards the south obscuring this part of the filament for a while. After the flare the filament was fragmented, but it reoccurred essentially at the same position as before the flare. The growing system of post-flare loops indicates that the field above the active region opened and subsequently reconnected (following the model by Kopp and Pneuman, 1976), but the field opening must have been accomplished only above the filament. This is also confirmed by the fact that the separation of the two bright Hα flare ribbons (at the footpoints of supposedly reconnected loops) was quite large since the flare onset, with $\sim 25\,000$ km distance between the outer edges (Švestka and Poletto, 1985).

The onset of the flare was described by Hoyng *et al.* (1981). The filament broadened and became diffuse near the site of the main flare emission at 20 : 45 UT and parted at 20 : 48 UT when the 8–20 Å X-ray emission (measured aboard the GOES-2 satellite) began to grow. By 20 : 50 : 38 UT the filament has broken into two distinct sections and at 20 : 54 : 50 UT several Hα patches reached kernel brightness. The flare entered its impulsive phase; this is described in the following section.

4. The Impulsive Phase

The study of many flares, mainly during the Solar Maximum Year 1979–1981, and chiefly by the Solar Maximum Mission, has shown that at least during 1980 virtually all flares of some importance had an impulsive phase. That phase is characterized by the following five main properties:

– The occurrence of impulsive bursts, both in the hard X-ray energy range, $E \gtrsim 20$ keV, and in the GHz microwave rage, $f \gtrsim 10$ GHz.

– The location of the hard X-ray burst emission in small, well defined areas, with characteristic diameters of the order of 3000 to 10^4 km. These areas, called flare *footpoints* or flare *kernels*, are best visible in medium and high energies ($E \gtrsim 15$ keV), but are also detectable in lower energies, after a subtle procedure of 'gradual background substraction' (De Jager and Boelee, 1984; De Jager *et al.*, 1984).

These first two properties indicate thick-target interactions of beams of electrons incident on the chromosphere (Duijveman, 1983).

Violent upward motions appear during the first few minutes of the impulsive phase; they are observed through shortward displayed spectral line components, mostly in the Ca XIX lines around 3.19 Å (Antonucci *et al.*, 1984). These velocity components range between 150 and 400 km s^{-1}; they are usually large in the first half minute of the

impulsive phase and decrease to smaller values in a few minutes time. On the average only one fifth of the Ca XIX emitting gas shows this upward motion component.

These phenomena are ascribed to convective upward motion of chromospheric gas heated to tens of MK.

– There is a gradual increase of the thermal energy content of the flare, reaching maximum value at the end of the impulsive phase (De Jager and Boelee, 1984).

This is interpreted as being the consequence of energy injection during the impulsive phase, principally by the electrons producing the hard X-ray bursts. Their energy is fed into the gradual phase component of the flare plasma by the convective motions described just earlier.

– There exists a high-temperature flare-plasma component during the very first part of the impulsive phase which is clearly indicated, both from Doppler widths of spectral lines (Antonucci *et al.*, 1984, 1985) and from spectral broad-band intensity ratios in the medium and high-energy spectral range (15–30 keV; Hoyng, 1982; Duijveman *et al.*, 1982; De Jager, 1985b). Hence the hot flare plasma has at that time a bi-thermal or non-thermal character. The temperature differences between the high-temperature and the 'low'-temperature components approach zero in a few minutes time, quasi-exponentially, with an *e*-folding time of ca. 1.5 min.

This behaviour is ascribed to kernel heating by beams of energetic particles. This heating, directly associated with the high-energy bursts, causes chromospheric ablation and results in the convective motions, just described (De Jager, 1985b). This upward moving gas, spreading around and above the flare footpoints, is proper to the gradual phase.

There are more properties of the impulsive phase; some of them have a fairly general character, but we think that the five listed above are the most essential ones. Let us examine these properties now for the 21 May, 1980 flare.

4.1. Impulsive bursts and footpoints

Figure 3 shows the time-development of the hard X-ray emission of the flare, as observed by the Hard X-Ray Burst Spectrometer (HXRBS) aboard SMM (Hoyng *et al.*, 1981). Only the first two peaks marked 1 and 2 are also clearly visible in the high-energy channel around 300 keV. These are the most energetic bursts. The later ones apparently involve electrons with smaller energies.

As shown first by Hoyng *et al.* (1981), these bursts are primarily associated with flare kernels, as appears from Figure 4, which is taken from a later, similar study, by Antonucci *et al.* (1985). There, the flare images are shown in low (3.5–8 keV) and high (16–30 keV) energies. The first high-energy image (20 : 55 : 15–20 : 55 : 35 UT) shows that there are two kernels, marked *A* and *B*. Hoyng *et al.* (1981) have shown that these kernels are situated at either side of, but very close to, the magnetic inversion line, which suggests that the kernels are loop footpoints. It is important to note that these kernels are *also* visible in the earliest low-energy images, being indicated even in images taken as early as 20 : 50 UT, see Figure 1. Hence, as it seems, the footpoints emission was already there before the onset of the hard X-ray bursts (Figure 3). The footpoints are

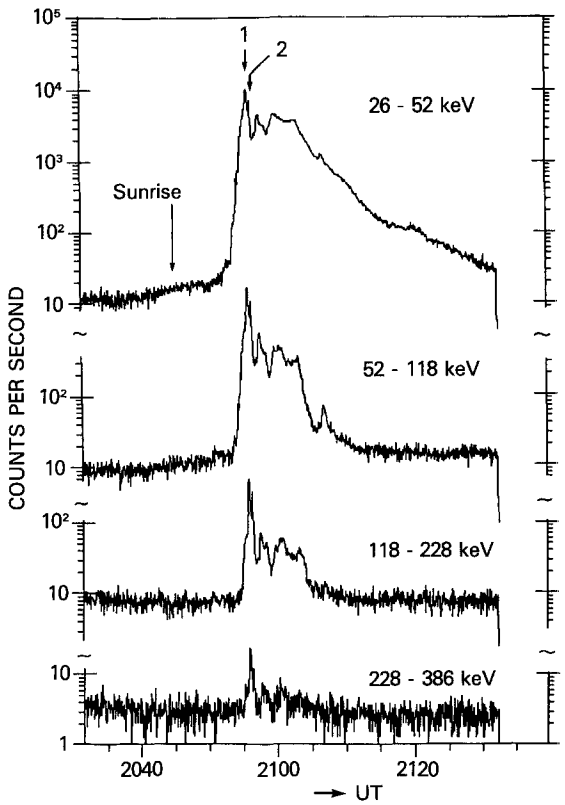

Fig. 3. Countrates during the 21 May, 1980 flare, observed in various energy channels of the Hard X-Ray Burst Spectrometer aboard SMM (From Hoyng *et al.*, 1981.)

seen particularly well in the image of 20 : 55 : 15 UT at burst maximum, an observation that applies to more flares seen by HXIS; it appears more clearly for the 21 May flare because of the high countrates of the flare. It is also important to note that at 20 : 55 : 35 UT, hence only half a minute later, the maximum countrate in low energy shifted to the central part of the loop: already after that short time interval the gradual phase component overruled the impulsive one, in low-energy images. After 21 : 57 UT the footpoints had disappeared also in high-energy pictures (Hoyng *et al.*, 1981). The existence of a third footpoint, initially mentioned by Hoyng *et al.* (1981), and called footpoint *C* by them, was not confirmed in the later research (Antonucci *et al.*, 1985), where calibration corrections were applied in a more refined way. Note, however (cf. Section 5), that a source of a coronal explosion occurs at the place of footpoint *C*.

The observations show therefore the existence of two footpoints in the flare, prior to and during the most energetic bursts, between 20 : 50 and 20 : 57 UT. Thereafter the gradual phase component was the most important one in the whole range of HXIS energies (3.5–30 keV).

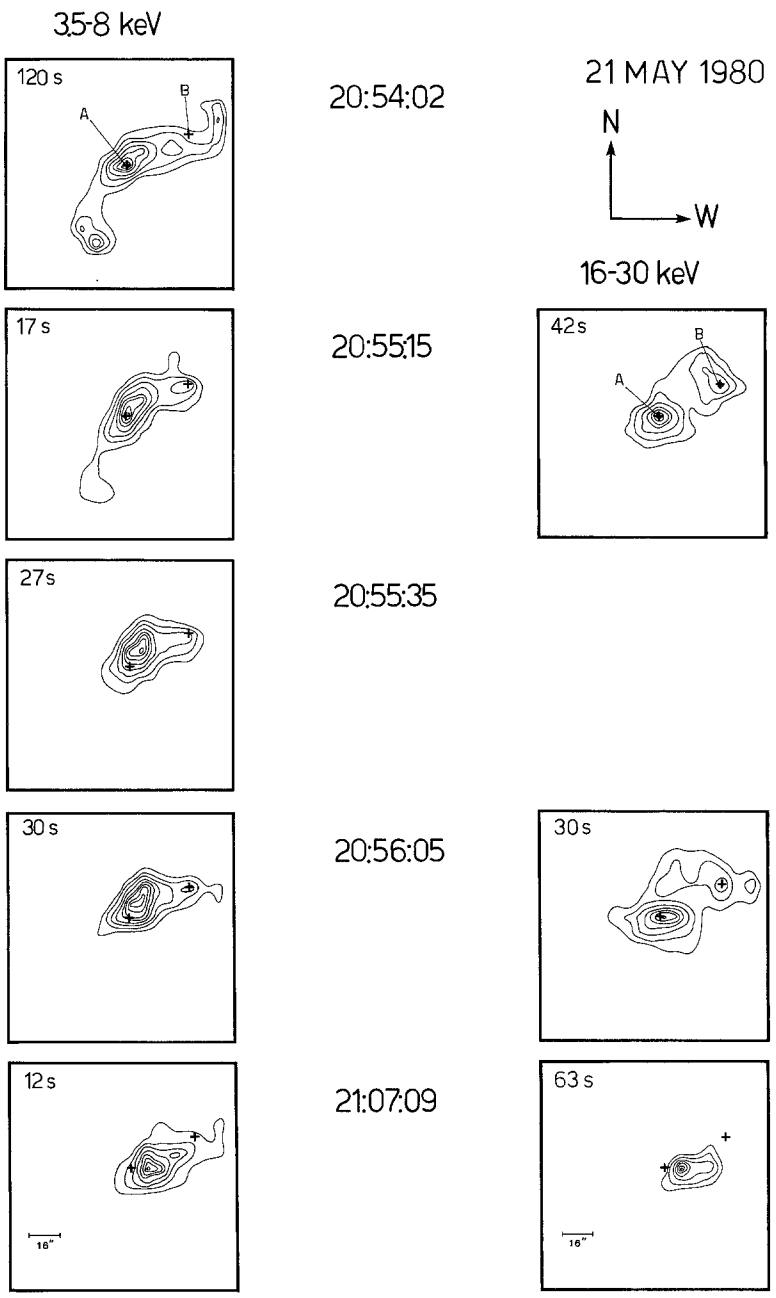

Fig. 4. X-ray images of the 21 May flare in the low-energy (3.5–8 keV) and high-energy (16–30 keV) ranges. The crosses *A* and *B* mark the two footpoints. The first high-energy image is averaged over the period covering the low-energy images at 20 : 55 : 15 and 20 : 55 : 35 UT. (From Antonucci *et al.*, 1985.)

4.2. THE HIGH-TEMPERATURE FLARE COMPONENT; UPWARD MOTIONS

Duijveman (1983) found from an analysis of HXIS observations in different energy channels that immediately after the occurrence of the first impulsive hard X-ray spikes (cf. Figure 3) the plasma showed evidence for a low-temperature component (20 MK) and a high-temperature one (40 MK). This has since been confirmed in various ways.

Figure 5, taken from Antonucci *et al.* (1985), shows the Ca XIX spectrum between 20 : 54 and 21 : 07 UT. Remarkable is the strong broadening of the lines in the initial phase, indicating ionic Doppler temperatures T_D of 130 MK at 20 : 53 : 59 UT, decreasing to 40 MK around 20 : 55 : 35 UT. In the later, fully gradual phase of the flare, at 21 : 07 UT, the ionic Doppler temperature (14 MK) is virtually equal to the electron temperature T_e (16 MK) derived from the intensity ratios and degrees of ionisation of the spectral lines. From a fit to line profiles, Bely-Dubau *et al.* (1982) found electron temperatures from 15 MK (21 : 00 UT) to 12 MK (21 : 20 UT).

These observations give rise to the following two comments. First, the ion-electron exchange time in typical flare conditions is short, of the order of a second or less (Duijveman and Hoyng, 1983; De Jager, 1985b) so that the thermalisation time is very short as compared to the time intervals that are relevant for the present discussion. Therefore, the ionic Doppler temperatures must be either electron temperatures of a hot flare plasma component (which could indicate that the flare plasma should be bi-thermal, or multi-thermal) or else the Doppler broadening indicates the presence of turbulent motions of the order of 220 ± 30 km s^{-1} at 20 : 54 UT. Antonucci *et al.* (1985) favour the latter possibility, while one of us (De Jager, 1985b) has given arguments for the bi-thermal interpretation. That this may be the case is supported by the broad-band HXIS intensity measurements (Hoyng, 1982). But only observations of a large number of lines, including those of other ions, with other molecular weights, should give the decisive answer.

Secondly, although the time dependence of the temperature difference $\Delta \log T$ ($= \log T_D - \log T_e$) is badly known, with only a few data points available, they do not contradict the results obtained for the 8 April, 1980 and 5 November, 1980 flares (De Jager, 1985b) that $\Delta \log T$ goes exponentially to zero with an e-folding time of about 1.5 min.

The time development of the line-of-sight convective motion component in the flare plasma is given in Figure 6 (marked v'), together with the emission measures (EM) for the undisplaced component (full-drawn line) and the upward moving component (broken line). This shows that the upward motions were 370 km s^{-1} at 20 : 55 : 13 UT, remained >300 km s^{-1} until 20 : 57 UT, and were ~ 150 km s^{-1} after 21 : 03 UT. The upward moving component apparently did not go to zero even as late as 21 : 05 UT, from which one infers that the footpoint heating continued till at least 21 : 05 UT. We will show later (Section 5) that the observations of chromospheric explosions in this flare support this inference. At 20 : 57 UT the emission measure of the displaced component was above one fourth of the undisplaced one. At 21 : 05 UT it had decreased to about one tenth, but it was not zero.

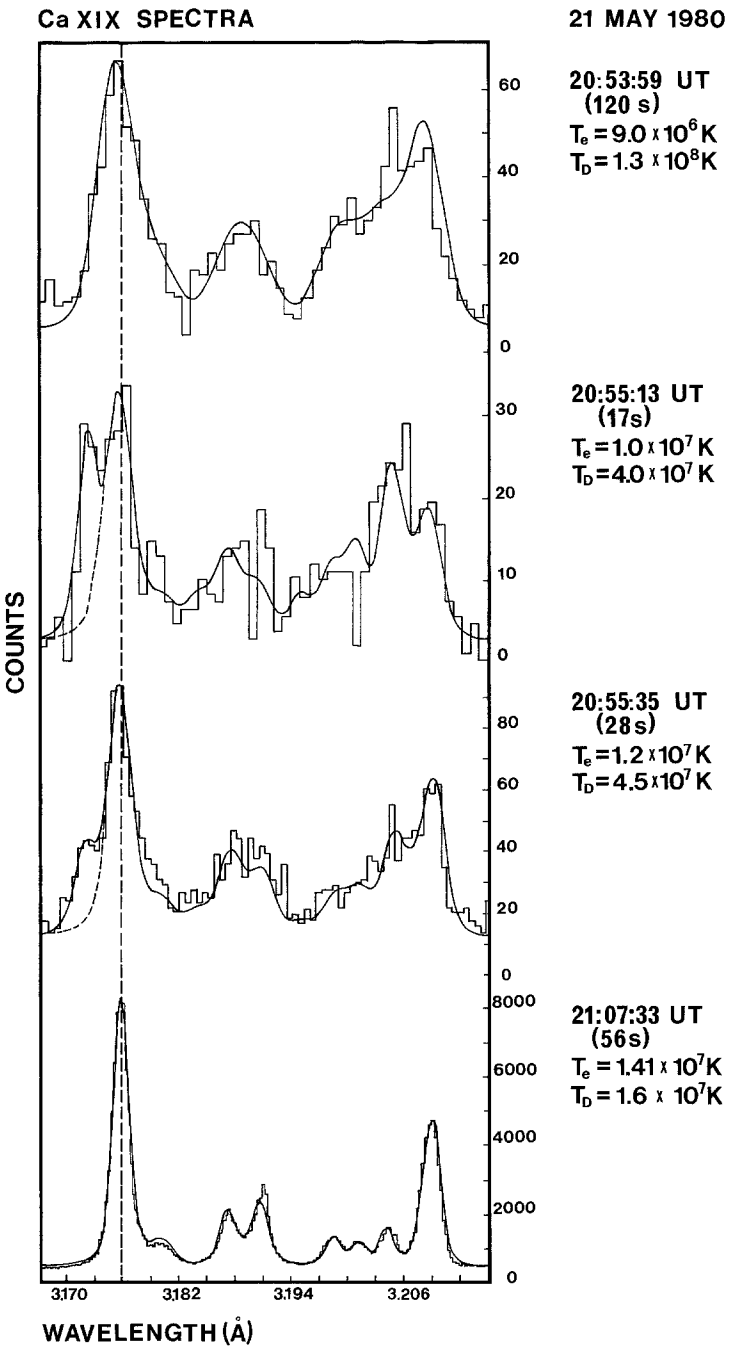

Fig. 5. Four Ca XIX spectra of the flare of 21 May, 1980, the first three being taken in the impulsive phase. The broadening and the shortward-shifted components are clearly visible. (From Antonucci *et al.*, 1985.)

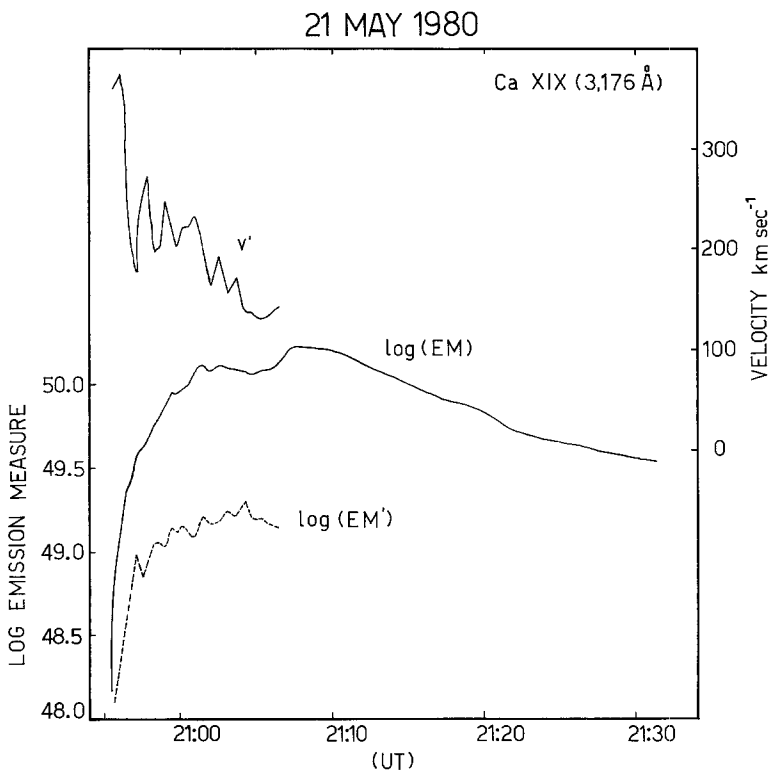

Fig. 6. Temporal evolution of the upward velocity component v', the emission measure for the kernel gas (EM) and for its displaced component (EM'). (From Antonucci *et al.*, 1985.)

4.3. Energies involved in the impulsive phase processes

In order to examine the energy balance of the flare, we have to compare three quantities: injection energy, convection energy, and thermal energy of the gradual phase.

4.3.1. *The Injection Energy*

The energy injected by an (assumed) beam of energetic electrons is determined from the energy spectrum of the hard X-ray burst, assuming thick-target interaction and taking for the spectrum of the incident electrons a power law (Duijveman *et al.*, 1983; Dennis *et al.*, 1985):

$$I(E) = AE^{-\gamma} \text{ photons cm}^{-2}\,\text{s}^{-1}\,\text{keV}^{-1}\,.$$

From $I(E)$ the energy spectrum is derived, and one can compute the energy contained in that beam for $E \geq E_0$, the cut-off energy. The choice of E_0 is often an arbitrary act.

Thus Duijveman *et al.* (1982), taking a cut-off of 16 keV, found for the spike at 20 : 56 UT (marked 1, 2 in Figure 3) an integrated energy of 3×10^{29} erg. However, as shown before, electron beam incidence continued after 20 : 57 UT, albeit to a lesser degree. Dennis *et al.* (1985) calculated for this flare over the whole impulsive phase an

integrated energy input of $(1 \pm 0.1) \times 10^{31}$ erg above $E_0 = 25$ keV, a value that seems nearer to the truth.

4.3.2. *The Convection Energy*

The second energy quantity one has to consider is that of the convected gas. We calculate this in the following way (cf. also De Jager, 1985b): according to Dennis *et al.* (1985) the kernels of the flare had a total area $A = 2.2 \times 10^{18}$ cm^2 and a volume $V = 25 \times 10^{26}$ cm^3. Since one fifth of the gas in this volume is moving upward, as shown by the spectral observations, the upward moving gas is contained in a column with a height $\frac{1}{5} \times V/A = 2600$ km, a value that may be identified with the depth of the ablated chromospheric 'hole'. Taking an average upward velocity (Figure 6) $v = 220$ km s^{-1} this means that the kernel gas needs 12 s to move over the height of the column. The kernel electron density is $n_e = 1.7 \times 10^{11}$ cm^{-3} (Dennis *et al.*, 1985). Hence, the production of hot gas by chromospheric ablation is $\dot{N} = \frac{1}{12} \times n_e \times \frac{1}{5} v = 6.9 \times 10^{36}$ electrons s^{-1}. Taking an exponential decrease of the production of high-temperature gas with an e-folding time of $\tau = 1.5$ min ($\simeq 100$ s), the total number of hot gas particles produced during the first, most violent, part of the impulsive phase is $N\tau = 6.9 \times 10^{38}$. The amount of thermal energy carried upward is hence $3N\tau kT$, and with $T = 4 \times 10^7$ K this yields 1.1×10^{31} erg, a quantity equal to that of the energy input by electron beams (with $E_0 = 25$ keV), as derived in Section 4.3.1.

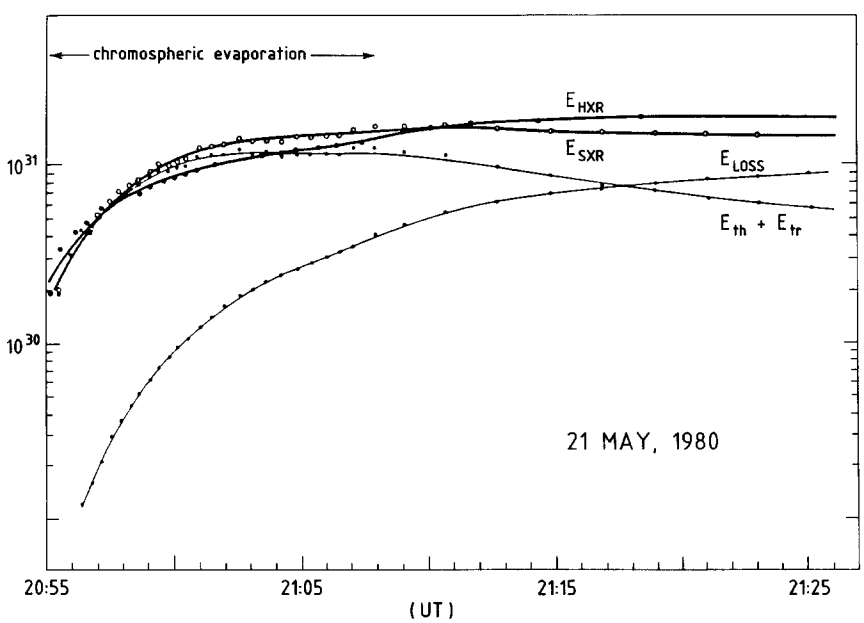

Fig. 7. Temporal variation, for the 21 May, 1980 flare, of the energy content of the low-energy X-ray emitting plasma E_{SXR}, the high-energy X-ray plasma ($E_0 = 25$ keV, E_{HXR}), the energy lost by radiation and conduction (E_{LOSS}), and the thermal and turbulent energies (E_{th}, E_{tr}). (From Antonucci *et al.*, 1984.)

4.3.3. *The Thermal Energy of the Gradual Phase*

The total thermal energy content of the flare in its gradual phase is easily derived from the emission measure Y, the area A (taking the volume $V = A^{3/2}$) and the kinetic temperature. However, energy losses should be taken into account, in a way first described by Antonucci *et al.* (1982). From detailed study of some flares, Antonucci *et al.* (1984, 1985) derived maximum values for E_{th} of 1 to 2×10^{31} erg, depending on the model assumed.

Figure 7 is a diagram due to Antonucci *et al.* (1984) showing for the 21 May flare the time development of E_{SXR}, the energy of the soft X-ray plasma; it is the sum of the thermal and turbulent energies, with radiative and conductive losses substracted. E_{HXR} is the energy contained in the high-energy flare plasma (> 25 keV). It is of the order of 2×10^{31} erg at 21:10 UT.

We conclude that in spite of some slight inconsistencies in the models used by various authors and in their basic assumptions, there is good order-of-magnitude equality between the electron beam energy input, the thermal energy convected upward, and the eventual thermal energy of the gradual phase plasma. All values are $\simeq 1$ to 2×10^{31} erg.

5. Transition to the Flare's Gradual Phase, Coronal Explosions

Let us take the values of Dennis *et al.* (1985; cf. also Wu *et al.*, 1986) for the parameters of the impulsive phase at the peak time of the soft (~ 5 keV) X-ray emission, 21:05 UT. The flare had at that time an area $A = 4 \times 10^{18}$ cm^2, a volume $V = 4 \times 10^{27}$ cm^3, a total thermal energy content of 7×10^{30} erg (slightly less than the value given in Figure 7), and an electron density of 8×10^{10} cm^{-3}. The energy content of the flare in the gradual phase has been acquired by footpoint heating and consequent ablation and convection, the latter with velocities $\simeq 200$–300 km s^{-1} in the first part of the impulsive phase and about 150 km s^{-1} at 21:05 UT.

What happens further with the convected plasma can be examined by studying the lateral motions. The coronal explosions for this flare were investigated by Lemmens and De Jager (1985). This is done (De Jager, 1985a) by determining for each pixel the time at which local intensity maximum is reached and by drawing isochrones connecting these times of local maximum.

There appear to be *two* explosions in this flare. The first one started at or before 20:58:30 UT, just after the first impulsive hard X-ray spikes (Figure 8) and was progressing outward: initially with a speed of about 100 km s^{-1}, then accelerating to ~ 350 km s^{-1} and, thereafter, decreasing in speed again, first to about 100 km s^{-1} and later to lesser values. The explosion started simultaneously in two small areas almost coinciding with the two footpoints A and C of the flare as defined by Hoyng *et al.* (1981). It is remarkable that footpoint B (see Figure 4) did not coincide with an explosion source.

Also the second explosion (Figure 6 of Lemmens and De Jager, 1985) started in the footpoints A and C, but it was less violent, with velocities rather of the order of tens

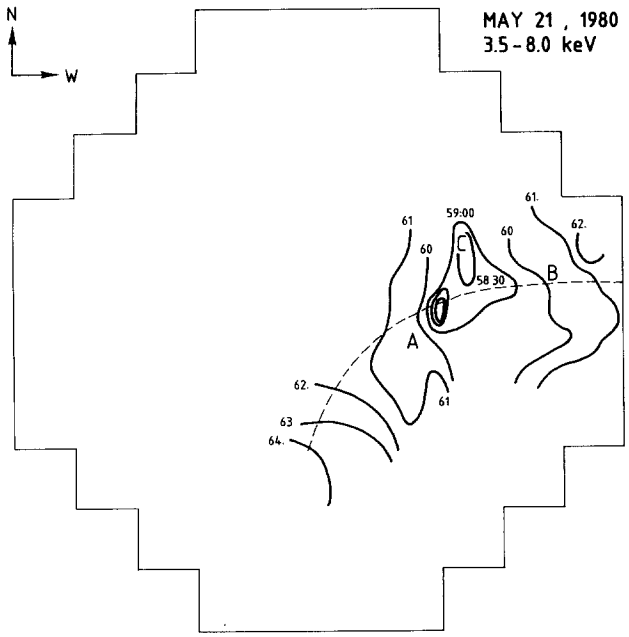

Fig. 8. Coronal explosion in the 21 May flare, observed in the low-energy HXIS channels (3.5–8.0 keV), after the impulsive spikes at 20 : 56–20 : 57 UT. The lines are isochrones labeled with the time in minutes after 20:00 UT. (From Lemmens and De Jager, 1985.)

of km s^{-1}. This second explosion was probably related to the burst complex at 21 : 00–21 : 03 UT, but it may also be associated with the spray that was seen in Hα since 21 : 50 UT (cf. Section 8).

The following interpretation has been proposed for the coronal explosions. Lemmens and De Jager suggest that they reflect the lateral outstreaming of gas initially convected upwards in the flare kernels. These authors showed for the 1980 November 12, 02 : 50 UT flare that the velocity variation can be mimiqued best by assuming flare plasma streaming, with conservation of mass, in cylindrical tubes which occupy a volume situated over the kernel and being larger than it. The fact that this kind of motion seems to be the case for any explosion observed so far (in contrast to the often assumed restricted streaming into and inside one loop connecting the footpoints) indicates that any flaring region must be a most complicated system of magnetic loops and should certainly not contain only one or a few distinct loops: a spaghetti-bundle model or a fanning-out fountain model look more probable. Also, reconnection between any of such loops in the course of a flare must be a normal process.

This interpretation may be supported by the observation of Antonucci *et al.* (1985) – cf. Figure 4 – that immediately after first kernel heating the center of gravity of the gradual emission component tended to move upward. The pictures at 21 : 07 UT in Figure 4 show a southward offset of the flare intensity maximum. But already at 20 : 57 UT the centroid of the emission had shifted southward by 5 arc sec (cf. Figure 9).

This indicates upward growth of the whole loop system, first described by Švestka *et al.* (1982a) and discussed in detail in the next section.

A possible consequence of this model had earlier been proposed by one of us (De Jager, 1985a): the upward moving component of the explosion becomes a magneto-hydrodynamical shock that may accelerate in less dense plasma, and then show up as a type II radioburst. A type II burst was indeed observed at Culgoora (Švestka *et al.*, 1982a) starting at 20 : 57 UT, close to the onset time of the first coronal explosion.

6. Growth of Post-Flare Loops

The shift of the maximum of brightness to the SW in Figure 4 shows the beginning of the growth of (post-) flare loops. Since the flare was at 13 S and 15 W, the shift to the SW reflects a growth in altitude in projection on the solar disk.

Figure 9, in its top, presents several images of the flare during more than two hours of its development. It is well-known that the post-flare loops are brightest at their tops (cf. e.g., Nolte *et al.*, 1979) so that there is little doubt that we image here the growth of the post-flare loops in the solar corona.

The central part of Figure 9 illustrates the time variation of temperature and emission measure in the brightest part of the flare imaged above. The electron temperature, determined from the flux ratio of HXIS bands 3 (8.0–11.5 keV) and 1 (3.5–5.5 keV) results here in much higher values than the temperature derived from line intensities and line profiles in Section 4.2. That is because the temperature here was deduced for the brightest part of the flare, whereas the line profiles and temperatures in Section 4.2. (Figure 5) represent averages over the whole flaring region.

The bottom part of Figure 9 shows the time variation of the distance d of the brightest portion of the loops from the $H_{\|} = 0$ line (Švestka and Poletto, 1985). For radial loops the real altitude would be 3.0 d. One can see that the growth of the flare loops in altitude was not continuous: the tops of the loops stayed for minutes at a given altitude before, quite abruptly, other loop tops began to appear above them. One may wonder if this was related to the second coronal explosion which lasted from 21 : 04 until 21 : 10 UT (Lemmens and De Jager 1985, Figure 6). A similar observation was made by Hinotori on 13 May, 1981, when the tops of flare loops stayed at the same altitude for 12 min (Tsuneta *et al.*, 1983: cf. Figure 14 in the paper by Dennis in this issue). Also in movies of post-flare loops in the Hα line one can sometimes see such abrupt jumps. Whereas, however, the jumps seen in Hα might have been due to effects of differences in the cooling of plasmas at different initial densities, the X-ray jumps are clearly related to the loops' excitation or formation. It is of interest that Forbes and Priest (1983) theoretically predicted the existence of multiple X-type neutral lines at several different altitudes above two-ribbon flares, where distended field lines may subsequently reconnect and thus produce new sets of loops at different higher altitudes.

The first 'jump', at 20 : 57 UT, apparently indicates the first formation of (post-) flare loops, probably through reconnection of earlier opened (distended) field lines (Kopp and Pneuman, 1976). The temperature at the top of these loops was close to 24 MK

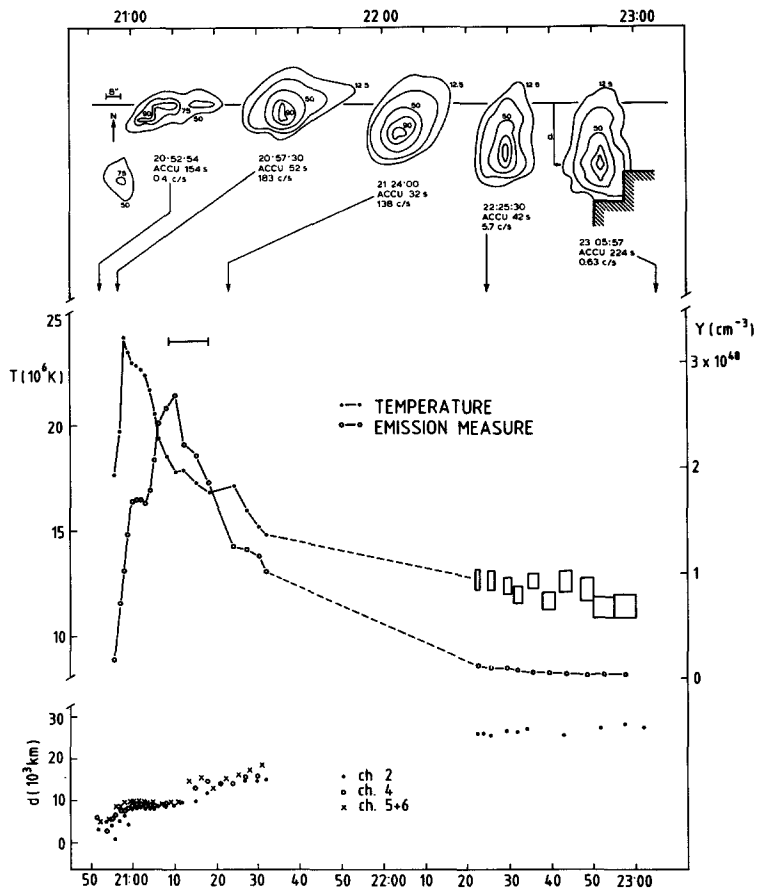

Fig. 9. Top: HXIS images of the flare of 21 May, 1980 in 3.5–8.0 keV X-rays (after Švestka *et al.*, 1982a). *Center*: temperature T and emision measure Y (per pixel of HXIS fine field of view) determined for the four brightest pixels from the ratio of HXIS bands 3 (8.0–11.5 keV) and 1 (3.5–5.5 keV). *Bottom*: the distance of the brightest part of the flare (tops of the loops) from the $H_{\parallel} = 0$ line, d, in projection on the disk, as determined from HXIS bands 2, 4, and 5 + 6. (After Švestka and Poletto, 1985.)

(Figure 9), but at least some of them must have cooled very fast, since the first Hα loops were seen at 21:00 UT. The cooling time of 3 min from $T \simeq 24$ MK to $T \simeq 10$ kK shows that the electron density might have been as high as 1.5×10^{12} cm^{-3} in the early formed loops.

Figure 10 shows an enlargement of the second abrupt rise in altitude that is evident at 21:12 UT in Figure 9 (Švestka and Poletto, 1985). It demonstrates clearly that the rise was first seen in the highest energy channel 6 (22–30 keV) with a later follow-up at lower energies. This can be interpreted as a new release of energy in a very small volume of plasma at extremely high temperature (a rise from 20 to 50 MK enhances the flux in HXIS channel 6 by a factor 2200, but only by a factor 3 in channel 1). A likely candidate for the process we observe here is the reconnection of field lines, in apparent

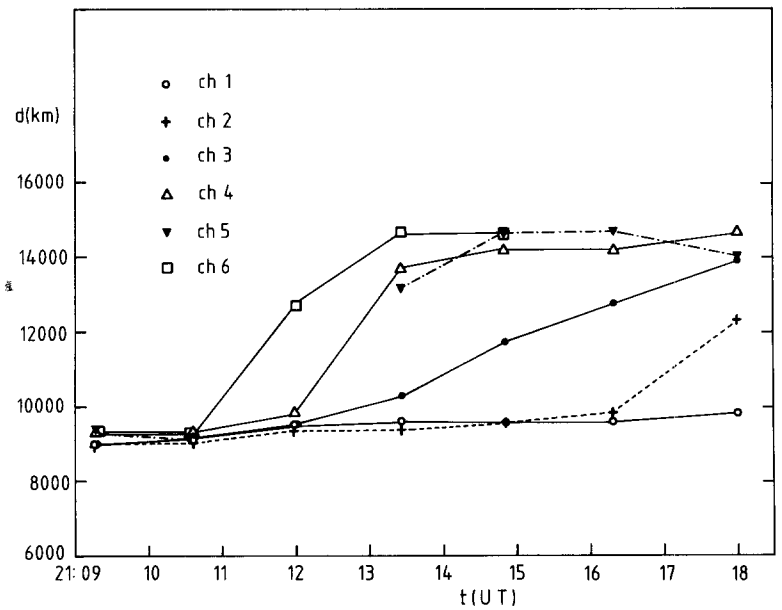

Fig. 10. The variation of d in HXIS channels 1 (3.5–5.5 keV) – 6 (22–30 keV) during the jump in altitude which occurred at 21 : 12 UT (cf. the bottom part of Figure 9; from Švestka and Poletto, 1985).

agreement with the Kopp and Pneuman (1976) model of the formation of post-flare loops (in the basic configuration suggested by Sturrock, 1968; and with the multiple neutral lines deduced by Forbes and Priest, 1983). Kopp and Poletto (1985) compared the observations with model predictions and have concluded that there is good evidence for magnetic reconnection to be directly witnessed in the corona during this flare.

The available data do not allow us to deduce a unique set of parameters for the new source of the energy release. However, a reasonable agreement with the observation is found for a source with a temperature of 50 MK from 21 : 08 through 21 : 13 UT, growing in size (supposedly as an arcade of loops was formed) and reaching an emission measure of 3×10^{45} cm^{-3} at the end of its development. Then the source cooled, and its emission measure was fast increasing (possibly through evaporation of chromospheric material into the new loops) to 3×10^{47} cm^{-3} at 21 : 17 UT, i.e., by two orders of magnitude during 4 min. Table I gives the estimated size of the new source of energy release at 21 : 13 UT for various (unknown) electron densities.

The new brightening at a higher altitude (43 000 km if the loops extended radially, but probably at 21 000 km as we will see in Section 7.1) occurred 23 min after the flare onset and 17 min after the maximum in the hard X-ray burst. Thus it represents an energy release late in the post-maximum phase of the flare, which gives direct evidence that, in two-ribbon flares, energy is still being released after the end of the impulsive phase.

The post-flare loops could be clearly seen in X-rays for two satellite orbits, up to 23 : 07 UT (2 hr and 15 min after the flare onset). At that time the loop temperature decreased from 24 MK to 12 MK and their altitude increased to $d = 28\,000$ km in

TABLE I

Size of the new source at 21:13:19 UT for various assumed electron densities

n_e (cm^{-3})	Volume (cm^3)	Radius (if source spherical) (km)
10^9	3.4×10^{27}	9330
10^{10}	3.4×10^{25}	2010
10^{11}	3.4×10^{23}	430
10^{12}	3.4×10^{21}	90

projection (most likely 41 000 km above the photosphere, cf. Section 7.1). Unfortunately, the SMM spacecraft did not look at the flare for the following two orbits. It came back to this active region only at 03:08 UT the next day, when the post-flare loops had completely disappeared. However, long enough integration of HXIS images revealed then another coronal structure above the flare region, which is discussed in the following section.

7. Post-Flare Coronal Arch

The very low background of HXIS made it possible to detect in X-rays large arch-like structures in the solar corona, which are formed, or become enhanced, after two-ribbon flares characterized by post-flare loops. Flares of other kinds apparently do not produce or affect these structures (Švestka, 1984a, b). The flare of 21 May 1980 was the first event, after which this new post-flare coronal phenomenon was detected (Švestka *et al.*, 1982a).

Figure 11 shows a series of images of the arch which became visible when the SMM returned to the flaring active region at 03:08 UT on May 22. All these images are half-an-hour integrations of an extremely weak structure: the peak countrate of the last image, at 06:36 UT, only slightly exceeded 1 count min^{-1} per pixel; yet this is still four times more than the average background noise in the 3.5–5.5 keV energy band of HXIS.

One can see that the brightest part (apparently the top) of the arch stayed in the same position from 03:20 UT (6.5 hr after the flare onset) till the end of the HXIS imaging period. Last images prior to the first one in Figure 11 are from 23:07 UT when the post-flare loops still fully dominated the field so that it was extremely difficult to distinguish the much weaker coronal arch. Nevertheless, a careful analysis made it possible to separate the brightest part (top) of the arch from the loops and the results are shown in Figure 12 (Hick and Švestka, 1985): since 23:02 UT the top of the arch was in the same position as in the much later images of Figure 11 (the righthand image). Prior to that, from the beginning of the orbit at 22:28 UT, the maximum was in a neighbouring pixel, but still at about the same altitude above the flare. If one follows the time development of the X-ray flux in these two pixels, one finds that the flux in the first pixel peaked at ~22:56 UT, whereas the other pixel peaked some 10 min later and since then remained the brightest pixel in the field.

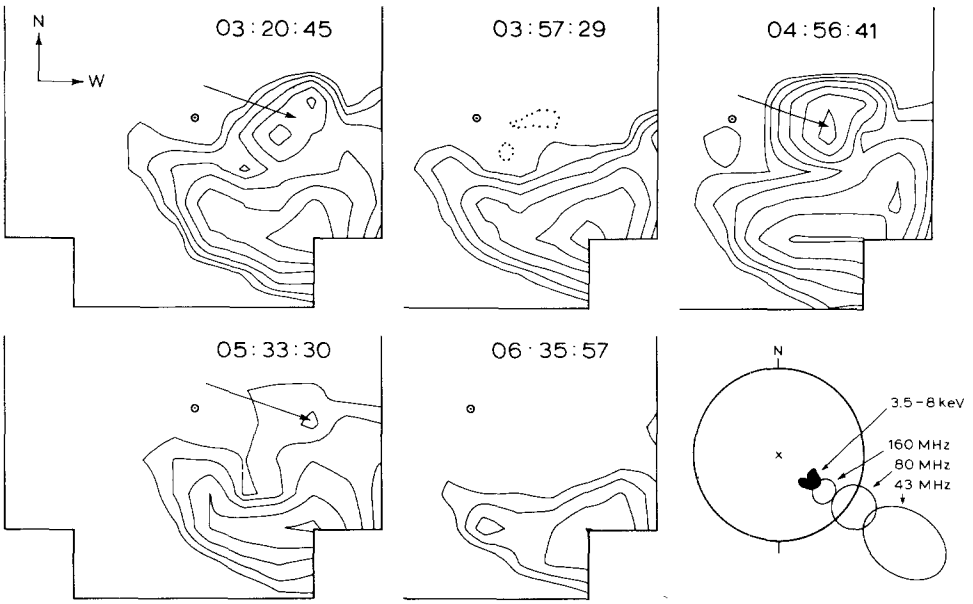

Fig. 11. X-ray contours of integrated images of the post-flare coronal arch observed on 22 May, 1980. Energy range 3.5–5.5 keV; HXIS coarse field of view, resolution 32 arc sec. The given times are mean times of 1525 s integrations. The position of the parent flare at 20 : 52 UT on 21 May (6.5 hr prior to the first image of the arch) is marked by dotted contours in the upper central image. Arrows point to a variable region below the arch discussed by Švestka *et al.* (1983; the reader is referred to this paper which analyses similar variations in another flare). The insert shows the relative position of the X-ray arch (black) and three radio images of the stationary type-I noise storm as seen at Culgoora at 03 : 20 UT on 22 May. (After Švestka, 1984b.)

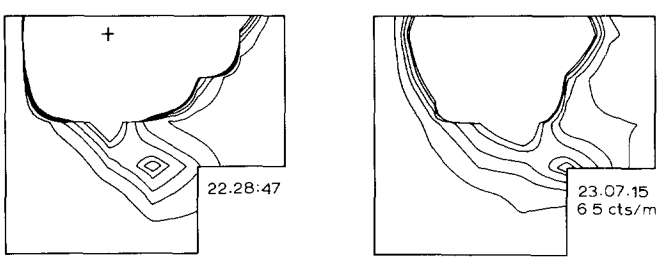

Fig. 12. X-ray contours during the SMM orbit next to the flare occurrence. HXIS coarse field of view, energy band 3.5–5.5 keV. The two images were recorded at respectively the beginning and end of the SMM orbit. (After Hick and Švestka, 1985.)

Thus the arch apparently consisted of at least two different structures which peaked in brightness at different times but stayed at a projected altitude of ~ 100 000 km above the $H_{\parallel} = 0$ line for more than 8 hr. Taking into account the spatial resolution of the HXIS coarse field of view (32 arc sec), the extreme upper speed limit for any motion of this arch is 1 km s^{-1} so that the arch was clearly a stationary structure. From this point of view it differs from other events of this kind, discovered later (Švestka,

1984a, b), in which the maxima of brightness moved upwards with speeds of 8–12 km s^{-1}.

The fact that HXIS could not detect the arch prior to 22 : 28 UT during the flare orbit does not necessarily imply that the arch did not exist at that time. During the flare, HXIS worked in its flare mode, yielding information only about the brightest X-ray features, which was done so in order to enhance the time resolution. Thus the arch, much weaker than the flare, simply was not imaged. In another event of this kind, on 6 November, 1980 (Švestka, 1984a) the coronal arch began to brighten at the flare onset, but reached the maximum of its brightness only $2^h\ 15^m$ later. This agrees well with the data presented here: the two components of the 21 May arch reached their maxima $2^h\ 06^m$ and $2^h\ 16^m$, respectively, after the beginning of the flare.

7.1. Associated Radio Emission

The radio spectrograph at Culgoora observed a type II metric burst associated with the flare, starting at 20 : 57 UT on May 21 and lasting until 21 : 57 UT. The possible association of this burst with the coronal explosion of 20 : 58 UT was mentioned in Section 5. Possibly since 21 : 10 UT, and definitely since 21 : 30 UT, a type IV burst was observed at 20–200 Mhz. Stewart, in Švestka *et al.* (1982a), assumes that the latter burst was stationary, but no position data is available until 23 : 16 UT when the heliograph started its observations. It was stationary for at least six hours after that. The burst was at first a mixture of a continuum and a noise storm, but it could be classified as a pure type I noise storm after 23 : 50 UT. The Culgoora heliograph could follow the noise storm until the end of the observing period at 05 : 10 UT on May 22.

As one can see in the insert in Figure 11, the type I noise storm radio emission was observed directly above the X-ray arch, so that the arch clearly images in X-rays the lowest part of the radio noise storm region. We can estimate the real altitudes of the radio images at various frequencies, since the radio emission is visible only at levels in the corona where the plasma frequency is lower that the radio frequency ν, i.e., above the level for which the electron density is

$$n_e = (\nu/9)^2 \times 10^6\ \mathrm{cm}^{-3}\,,$$

with ν in MHz. If the whole structure in Figure 11 extended in the radial direction above the active region, the found densities would exceed by factors 30 to 100 the electron densities n_0 in the quiet corona. One has to incline the whole structure by 20° to 30° to the south–west to get $n_e/n_0 \simeq 10$ which is more reasonable for an active region (Hick and Švestka, 1985). This inclination is also suggested by coronagraphic observations of the active region on the western limb (Wagner, in Švestka *et al.*, 1982a): the coronagraph showed a (projected) southward tilt of roughly 20° from the vertical corresponding to a real south-west tilt of $\sim 25°$.

Švestka and Poletto (1985) have demonstrated (in their Figure 2) that the post-flare loops grew exactly in the direction (PA = 225°) where the Culgoora images of the radio storm and the HXIS X-ray images of the arch were projected. Thus, since it is reasonable to believe that the arch is an upper product of the same reconnection

processes that lead to the formation of the post-flare loops (cf. Section 4.7), we may assume that the post-flare loops, the X-ray arch, and the radio noise storm all extended in the same spatial direction, tilted by $\sim 25°$ to the south-west. In that case the brightest part of the arch was at an altitude of 145 000 km above the photosphere; the height of the flare loops was 21 000 km after the abrupt rise at 21 : 12 UT and 41 000 km at the end of HXIS observations at 23 : 07 UT.

7.2. Physical Parameters of the Arch

Hick and Švestka (1985) have determined the temperature T and emission measure Y at the top of the arch by comparing X-ray fluxes in HXIS bands 2 (5.5–8.0 keV) and 1 (3.5–5.5 keV). At the time of its maximum brightness ($\sim 23 : 00$ UT) the arch temperature was found to be 6.3 ($\pm$ 1.3) MK. In the same phase of development the temperature T in the well-observed second arch of November 6 (Švestka, 1984a) was ~ 13.4 MK. In that arch, T peaked 1 hr 20 min earlier reaching ~ 14.5 MK and decreased 4 hr later to ~ 8.5 MK. In contrast to it, T remained remarkably constant in the May arch: $T \approx 7.1$ ($\pm$ 1.8) MK at 03 : 40 UT and $T \approx 6.4$ ($\pm$ 1.3) MK at 05 : 20 UT on May 22. This has been also confirmed by temperature determinations from the Ca XIX line complex observed by the Bent Crystal Spectrometer on board of the SMM. Acton, Gabriel and Rapley (in Švestka *et al.*, 1982a) found $T = 7.0$ ($\pm$ 0.5) MK at 03 : 25 UT, 6.0 ($\pm$ 0.5) MK at 03 : 53 UT, and 6.4 ($\pm$ 0.5) MK at 05 : 19 UT.

Taking $T = 6.3$ MK, the emission measure at 23 : 00 UT was $Y \approx 1.0 \times 10^{47}$ cm^{-3} per pixel (of the coarse field of view). Assuming that the linear thickness of the arch at the location of the maximum of brightness was of the same order as its altitude, $l \simeq h \simeq 145\,000$ km, we find an electron density $n_e \simeq 1.1 \times 10^9$ cm^{-3} and the corresponding energy density $\varepsilon = 3n_e kT \simeq 2.9$ erg cm^{-3}. With the emitting volume estimated to $V \simeq 5.0 \times 10^{29}$ cm^{-3} the total energy content was $E = V\varepsilon \simeq 1.4 \times 10^{30}$ erg (which is about one tenth of the initial energy input into the flare – Section 4.3), and the total mass $M \simeq 8.9 \times 10^{14}$ g.

In comparison with the second arch of November 6, the post-flare coronal structure of 21/22 May was a weak event. The corresponding values for the (much brighter) November arch were (Švestka, 1984a) $E \simeq 1.2 \times 10^{31}$ erg and $M \simeq 4.4 \times 10^{15}$ g. Yet, in both cases the arch energy is still a significant fraction of the energy of the parent flare and the mass of the arch is comparable with the mass of an active region filament. The values of E and M are also of the order of magnitude of the energy and mass values found for coronal transients.

7.3. Proposed Interpretation

Švestka *et al.* (1982a) have tried to explain the arches as a byproduct of the Kopp and Pneuman (1976) model for two-ribbon flares, modified for sheared field lines by Anzer and Pneuman (1982). Figure 13 illustrates this idea.

Prior to the flare (Figure 13(a)) a system of sheared active region loops bridges the $H_{\parallel} = 0$ line. When the flare starts, these loops are extended high into the corona. At a certain level a reconnection process starts (Figure 13(b)) due to the resulting

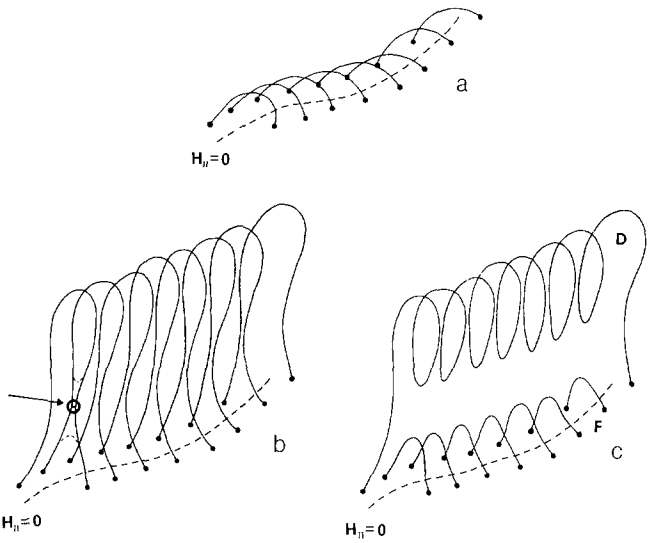

Fig. 13. If the pre-flare magnetic field is sheared (a) and is extended upwards at the onset of the flare (b), reconnection occurs between neighboring field lines (arrow in (b)). As a result we get then less sheared post-flare loops below (*F* in (c)), while the upper disconnected loops (*D* in (c)) become interconnected along the $H_{\parallel} = 0$ line. This may schematically represent the post-flare arch. (From Švestka *et al.*, 1982a.)

unbalance between the magnetic pressure and gas pressure, leading to the formation of less sheared post-flare loops in the low corona and another system of reconnected fieldlines above.

In the original Kopp and Pneuman model the field lines open. This, however, can never be achieved if the field is sheared, as has been pointed out by Aly (1984). In that case the dynamical situation of the system cannot lead to an open field for the simple reason that such a configuration is a state of maximal energy for the force-free field. However, the field opening can be closely approached as we schematically indicated in Figure 13(b); then the reconnection gives rise to systems of coil-like magnetic fieldlines extending along the $H_{\parallel} = 0$ line of which one is schematically shown in Figure 13(c).

There is a long sequence of such reconnecting coils that merge, mix, partly reconnect, and eventually give rise to a very complex magnetic field formation above the flare site in which plasma, excited in the reconnection process, is confined and seen in X-rays as the post-flare arch.

The fact that solely the two-ribbon flares, with their growing systems of loops, give rise to these arches, greatly supports this interpretation. Another strong supporting fact is the observed propagation of the growing loops and the extension of the arch and radio type I noise storm on 21/22 May along the same direction of $PA = 225°$ (cf. Section 7.2). The main objection against this model is the stationarity of the arch. In the original picture by Anzer and Pneuman (1982) the sequentially reconnected coils move steadily upwards, driven by magnetic pressure from below. To keep the whole structure fixed at a constant altitude for eight or more hours needs some force that

compensates for this drive. It has been suggested that this braking agent is related to the magnetic complexity of the arch which orginates through reconnections between the sequential coils and eventually creates a self-supporting post-flare structure above the active region.

Švestka *et al.* (1982a) assumed that the plasma heated during the reconnection process, and particles accelerated in the reconnection, propagate into the complex field of the arch, are trapped there, and produce the observed X-ray emission. Achterberg and Kuipers (1984), on the other hand, have suggested that the diffusion of electrons with energies in excess of 100 keV out of the flaring loops in the solar corona are the energy source of the observed X-ray and radio emission. The diffusion agent is low-frequency magnetic turbulence in the lower corona which appears to play a more important role than regular drifts for the cross-field electron transport.

These authors did not try to explain the origin of the loops. The sequential reconnection process suggested by Kopp and Pneuman seems necessary, because the growth of post-flare loops can last up to 11 hr (cf. Nolte *et al.*, 1979). Therefore, heating and acceleration processes during the reconnection have to be taken into account. Nevertheless, the interpretation proposed by Achterberg and Kuijpers may perhaps help to understand the propagation of accelerated electrons across magnetic field lines into the post-flare arch.

7.5. Origin of the Arch

In the November event (Švestka, 1984a) the whole arch began to brighten at the very onset of the flare, reaching maximum brightness about 2 hr 15 min later, but at the same time the maximum of brightness was steadily moving upwards. This has been interpreted as the filling-up of a pre-existing arch with heated plasma while a new arch-like structure was being formed from below. It took about six hours before the moving structure reached an altitude of $\sim 150\,000$ km, the altitude of the stationary March arch.

The May arch apparently reached this altitude in less than 1.5 hr. Thus the average rise velocity must have been higher than 17 km s^{-1} if starting at $< 50\,000$ km altitude (as on November 6). Since we have no data about the arch for the first 1.5 hr after the flare onset, such a rise can neither be verified nor excluded.

It is, of course, also possible that the arch was built up very fast at the very onset of the flare as a counterpart of a coronal transient. We will see in Section 8 that there was no filament eruption in the May 21 flare: still a part of the magnetic field above the filament might have risen and create the arch near the time of the flare onset. This elevated structure would then be further enhanced by the long-lasting reconnection process schematically shown in Figure 13.

An alternative possibility is that the arch was a pre-existing structure in the corona, which just brightened when the flare appeared below it, as was the case in all three arches on November 6/7. But in all these three events there had been an earlier two-ribbon flare which could be held responsible for the creation of the pre-existing arch. No such flare preceded the flare event of May 21 (no significant activity at all preceded the May 21 flare, cf. Schadee *et al.*, 1983).

Nevertheless, as we saw in Figure 2, there was a leakage of plasma from the active region into interplanetary space prior to the flare, possibly associated with the semi-permanent weak activity along the filament channel (cf. Section 1). Since we know very little about the nature of the arch, one cannot exclude that its basic magnetic structure was also built up during this pre-flare period.

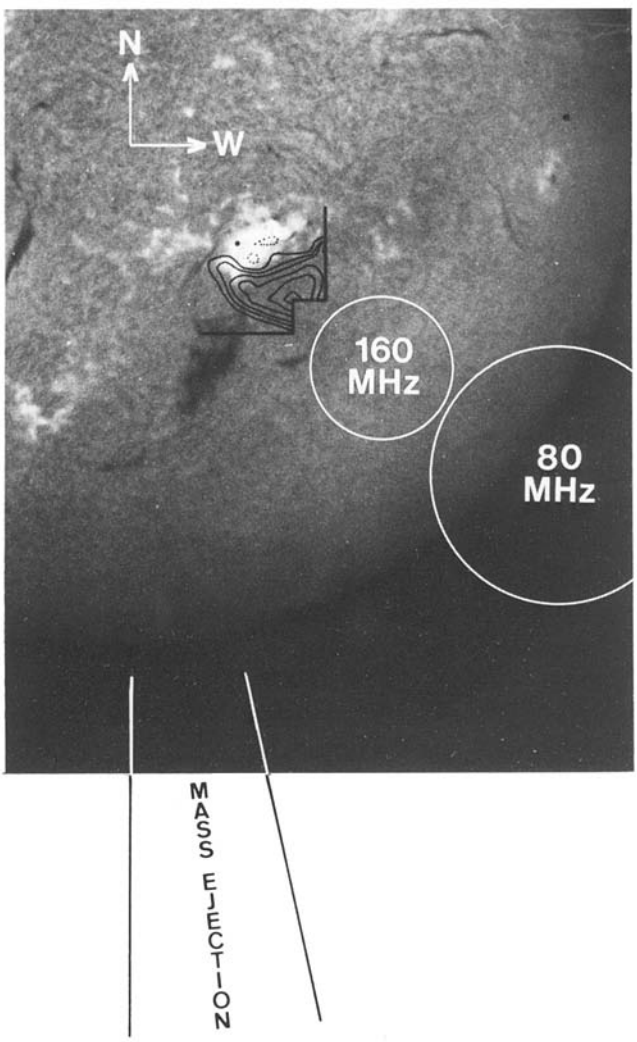

Fig. 14. Hα image of the Sun (Haleakala) at 21:20 UT on 21 May, 1980, showing the two-ribbon flare (white) and the associated dark spray (black). Projected on this image is the X-ray post-flare arch from Figure 12 (HXIS) and sites of the type I noise storm at 160 and 80 MHz (Culgoora) at 03:20 UT on 22 May. The cone of the mass ejection (Solwind, NRL) is shown at the bottom. (From McCabe *et al.*, 1985.)

8. Associated Mass Ejection

The NRL-Solwind coronagraph aboard the P78–1 satellite revealed a very bright and narrow feature in the corona propagating southward ($PA \simeq 180$–$192°$; Howard and Sheeley in McCabe *et al.*, 1985). The feature was first seen at 21:43 UT (53 min after the flare onset) and its leading edge reached 6.5 $R_\odot$ at 23:19 UT. The average speed of its propagation in projection on the plane of sky was 420 km s^{-1}.

Further information can be obtained about this mass ejection from the viewpoint of the zodiacal light photometers on board the Helios A spacecraft (Jackson in McCabe *et al.*, 1985). From both the Solwind viewpoint (at Earth) and the Helios viewpoint (about 30° east of the Sun–Earth line), the primary mass of the ejection was limited to a narrow angular extent moving southward of the Sun. The real speed of propagation in space, deduced from a comparison of the Solwind and Helios data was $\gtrsim 670$ km s^{-1}.

Under the assumption that the mass ejection originated in the flare, the direction disagrees by $\sim 40°$ from the direction expected if the flare filament erupted and produced the observed transient. The mass ejection should then extend approximately along the same direction as the X-ray arch and the radio noise storm (cf. Figure 14). However, as McCabe *et al.* (1985) have emphasized, the active region filament never erupted, and did not disappear. Instead, Hα-emitting material was ejected from the south–eastern end of the filament channel in the form of a spray at 21:05:20 UT (cf. Figure 14). The observed mass ejection was seen in the prolongation of the path of this spray, which apparently was the real source of the recorded coronal transient in this particular case.

The coexistence of stationary post-flare coronal structures (X-ray arches) and fast moving mass ejecta (coronal transients) in the post-flare corona poses a serious problem. In this event the coexistence can be easily understood: the mass ejection went through a narrow cone in another direction than where the stationary X-ray and radio structures were seen. But some other events are more complex: on 6 November, 1980, e.g., at 03:30 UT, Helios A (Jackson, private communication) and Culgoora (Stewart, private communication) clearly evidenced the presence of a very extensive transient. This has also been confirmed in later images by Solwind of the post-flare corona (Howard and Sheeley in McCabe *et al.*, 1985). Still, this flare also produced (or revived) a giant semi-stationary arch staying above the active region for more than 11 hr (Švestka, 1984a). We do not understand yet what really happens in the flaring and post-flare corona in such a case, but this problem is actually an old one: as early as in 1961, Pick distinguished between the first and second part of a radio type IV burst, of which part one corresponds to a moving type IV and part two to a stationary component of the same burst. An excellent example was imaged by Wild (1969) on 22 November, 1968. What we see here, appear to be X-ray images of the 'part two' which has developed into a noise storm.

The flare was a source of high-energy particles recorded in space. Helios A, at 0.35 AU from the Sun, yielded the following maximum fluxes (Wibberenz, private

communication):

0.8–2.0 MeV electrons: $5 \times 10^3\ m^{-2}\ s^{-1}\ sr^{-1}\ MeV^{-1}$;

3.8–12.6 MeV protons: $1 \times 10^4\ m^{-2}\ s^{-1}\ sr^{-1}\ MeV^{-1}$;

27–37 MeV protons: $2 \times 10^2\ m^{-2}\ s^{-1}\ sr^{-1}\ MeV^{-1}$;

27–37 MeV helium nuclei: no recognizable flux.

A minor shock wave from the flare hit Helios A at ~21 UT on 22 May; the time difference of ~24 hr corresponds to the mean speed of propagation of ~590 km s^{-1} (Sheeley *et al.*, 1984).

9. Final Scenario

From all these data we may suggest the following scenario for the flare of 21 May, 1980.

For more than 30 hr prior to the flare, the active region filament was greatly activated and X-ray images gave evidence for the existence of plasma with temperature in excess of 10 MK along the filament channel; or, alternatively, for intermittent, but very frequent acceleration processes near the $H_{\parallel} = 0$ line. It is likely that the weak mass-flow imaged by Helios A above 16 $R_{\odot}$ over the active region at that time was linked to this filament activity (Section 2). No important flares, however, did occur during that period.

A possible pre-flare X-ray brightening appeared at the flare site 90 min before the flare, with the X-ray flux growing by an order of magnitude during this period. An intense X-ray flare precursor was definitely present for $\gtrsim 6$ min before the flare onset (Section 3).

Strong downward motions appeared at the west end of the filament about 2 hr before the flare. At the same time, a kink developed in the middle of the filament, very close to the main site of the brightening in the flare. These destabilisations of the filament seemed to be linked to changes in the magnetic field first detected 80 min prior to the flare: a newly emerging flux compressed the existing flux below the kink, where a small new sunspot began to be seen (Section 3).

By 20 : 50 UT the filament had broken into two distinct parts at the site of the kink and the flare began to develop, supposedly through excitation of some coronal loops at this site and by opening (extending) of magnetic fieldlines at higher altitudes. Since the filament did not erupt (Section 8), the field opening must have been accomplished only above the filament, leaving the lower loop system, containing the filament, closed (Section 3). At that time already, the first faint indications of footpoint heating appeared (Figure 1; Section 4.1).

At the peak of the flare-associated hard X-ray burst, at 20 : 55 UT, hard X-ray images showed two distinct kernels of emission at opposite sides of the $H_{\parallel} = 0$ line: obviously the footpoints of an excited flare loop in which accelerated electrons produced thick-target X-ray emission (Section 4.1). Shortly before that, profiles of the Ca XIX lines showed remarkable broadening which can be interpreted either by turbulent motions

(with $\bar{v} \simeq 220$ km s^{-1} at 20 : 54 UT) or by a multi-thermal structure (with the hot component as hot as 130 MK at the very beginning). Chromospheric evaporation manifested itself through convective upward motions since the time of the hard X-ray peak (370 km s^{-1} at 20 : 55 : 13 UT), and the motions were still present ten minutes later which implies that even at that time the footpoint heating still continued (Section 4.2). However, the thermal gradual phase component dominated the X-ray images since 20 : 57 UT (Section 4.1).

The energy involved in the impulsive phase processes can be estimated to 1 to 2×10^{31} erg (Section 4.3).

Shortly after the peak of the impulsive phase, at or before 20 : 58 : 30 UT, a coronal explosion was detected in X-rays, with initial lateral speed of 100 km s^{-1} accelerating to ~ 350 km s^{-1} and decreasing thereafter. It might have been the lateral component of a wave of which the upward moving component transformed into a shock wave that manifested itself as a type II radioburst high in the solar corona (starting at 20 : 57 UT) (Section 5).

A second coronal explosion started at about 21 : 04 UT and could perhaps be associated with the spray seen in Hα since 21 : 05 UT (Sections 5 and 8).

At 20 : 57 UT X-ray images gave the first evidence of the existence of (post-) flare loops. In Hα, these loops were first seen at 21 : 00 UT which indicates that the electron density in the first (lowest) loops was $\leq 10^{12}$ cm^{-3}. The loops grew upwards, but the growth was not continuous: after staying for a while at a constant height, new loops began to appear abruptly at a higher altitude. One of these jumps in altitude, at 21 : 12 UT, gives evidence for a late release of energy high in the corona in a very small and extremely hot volume which may be most likely a product of field-line reconnection. This tends to support strongly the model of Kopp and Pneuman (1976) in which successive reconnections of earlier opened field lines produce the post-flare loops (Section 6).

About 1 hr after the flare onset the Solwind coronagraph began to image the mass ejection coming from the flare. Later on, its images were also obtained by Helios A from a different viewpoint. These observations show that the mass ejection was in the prolongation of the path of a powerful spray that was ejected at 21 : 05 UT from the south–eastern end of the filament channel, while the filament itself did not erupt (Section 8).

From 21 : 30 UT, Culgoora observed a stationary type IV burst associated with the flare, which changed into a type I noise storm at about 23 : 50 UT. From 1.5 hr after the flare, X-ray images revealed the existence of a giant coronal arch just below the radio noise-storm region. The arch extended along the filament channel over the active region to an altitude of $\sim 150\,000$ km. As the radio noise storm above it, the arch was completely stationary and stayed at the same altitude for more than 8 hr, slowly decaying in brightness (Section 7.1). Its energy content is estimated to be 1.4×10^{30} erg and its total mass 9×10^{14} g (Section 7.2). It is suggested that the arch was the upper product of the reconnection process that gave rise to the post-flare loops below (Section 7.3).

We believe that the results obtained for this particularly well observed flare have

extended our knowledge of the flare phenomenon in several important points. However, on the other hand, the observations also show how complicated the flare process actually is. Let us give here just two very brief examples.

In another paper in this issue, Bryan Dennis describes and discusses the characteristics of the Hinotori flares of classes *B* and *C*. The present flare, without any doubt, was both a class *B* (with emission at footpoints) and a class *C* (with emission high in the corona). Thus it belonged to the 'controversial events' mentioned by Dennis and we have some doubts whether oversimplified classifications can really help to understand flares.

Another believe is that two-ribbon flares and coronal mass ejections follow the eruption of a filament. Well, clearly, as in this flare, the eruptive field changes can occur entirely above the filament channel, leaving the filament in its preflare position. Still, the filament did not stay intact: it became fragmented and a powerful spray erupted near its eastern end some five minutes after the maximum of the flare impulsive phase.

One can see that variations in the altitude at which the field opens (erupts) can clearly produce a great variety of consequent flare configurations in the corona. And that is a variation of only one parameter in the flare process, and only in one kind of the flare phenomenon: the two-ribbon (dynamic) flares. We do not dare to go deeper into this problem here, but theoreticians should give some thought to it when modelling 'a flare'.

Acknowledgements

The extraordinarily rich set of space and ground-based data on this flare was obtained during an interval of coordinated observations organized by the Flare Build-up Study Project of the Solar Maximum Year. Thanks are due to all who participated in it and to the FBS coordinator Dr. Paul Simon in Meudon.

We are obliged to Hans Braun in Utrecht for his skilfull help when preparing the illustrations.

References

Achterberg, A. and Kuijpers, J.: 1984, *Astron. Astrophys.* **130**, 111.
Aly, J. J.: 1984, preprint.
Antonucci, E.: 1982, *Mem. Soc. Astron. Ital.* **53**, 495.
Antonucci, E. and Dennis, B. R.: 1983, *Solar Phys.* **86**, 67.
Antonucci, E., Gabriel, A. H., Acton, L. W., Culhane, J. L., Doyle, J. G., Leibacher, J. W., Machado, M. E., and Rapley, C. G.: 1982, *Solar Phys.* **78**, 107.
Antonucci, E., Gabriel, A. H., and Dennis, B. R.: 1984, *Astrophys. J.* **287**, 917.
Antonucci, E., Dennis, B. R., Gabriel, A. H., and Simnett, G. M.: 1985, *Solar Phys.* **96**, 129.
Anzer, U. and Pneuman, G. W.: 1982, *Solar Phys.* **79**, 129.
Bely-Dubau, F., Dubau, J., Faucher, F., Gabriel, A. H., Loulegrue, M., Steenman-Clark, L., Volonté, S., Antonucci, E., Rapley, C. G.: 1982, *Monthly Notices Roy. Astron. Soc.* **201**, 1155.
De Jager, C.: 1985a, *Solar Phys.* **96**, 143.
De Jager, C.: 1985b, *Solar Phys.* **98**, 267.
De Jager, C. and Boelee, A.: 1984, *Solar Phys.* **92**, 227.
De Jager, C., Boelee, A., and Rust, D. M.: 1984, *Solar Phys.* **92**, 245.

De Jager, C., Machado, M. E., Schadee, A., Strong, K. T., Švestka, Z., Woodgate, B. E., and van Tend,W.: 1983, *Solar Phys.* **84**, 205.

Dennis, B. R., Lemen, J. and Simnett, G.: 1985, *The Relationship between Hard and Soft X-Rays in Flares Observed with the Solar Maximum Mission during 1980*, preprint, also reproduced in Chapter V of SMM Workshop Proceedings.

Duijveman, A.: 1983, *Solar Phys.* **84**, 189.

Duijveman, A. and Hoyng, P.: 1983, *Solar Phys.* **86**, 279.

Duijveman, A., Hoyng, P., and Machado, M. E.: 1982, *Solar Phys.* **81**, 137.

Forbes, T. G. and Priest, E. R.: 1983, *Solar Phys.* **84**, 169.

Gaizauskas, V.: 1985, in *Proceedings of the NASA-SMM Workshop on Solar Flares,* Section 5, Chapter 3.

Harvey, J. W.: 1983, *Adv. Space Res.* **2**, No. 11, 31.

Hick, P. and Švestka, Z.: 1985, *Solar Phys.* (in press).

Hoyng, P.: 1982, *The Observatory* **102**, 119.

Hoyng, P., Duijveman, A., Machado, M. E., Rust, D. M., Švestka, Z., Boelee, A., de Jager, C., Frost, K. J., Lafleur, H., Simnett, G. M., van Beek, H. F., and Woodgate, B. E.: 1981, *Astrophys. J.* **246**, L155.

Jackson, B. V., Schadee, A., and Švestka, Z.: 1985 (in preparation).

Kopp, R. A. and Pneuman, G. W.: 1976, *Solar Phys.* **50**, 85.

Kopp, R. A. and Poletto, G.: 1985, in D. Neidig (ed.), *Proc. of Sac. Peak Summer Meeting on Low-Temperature Flare Plasma*, in press.

Kuperus, M. and van Tend, W.: 1981, *Solar Phys.* **71**, 125.

Lemmens, A. and de Jager, C.: 1985, *Solar Phys.* (submitted).

McCabe, M. K., Švestka, Z, Howard, R. A., Jackson, B. V., and Sheeley, N. L., Jr.: 1985, *Solar Phys.* (submitted).

Mewe, R., Gronenschild, E. H. B. M., and van den Oord, G. H. J.: 1985, Astron. *Astrophys. Suppl.* (in press).

Nolte, J. T., Gerassimenko, M., Krieger, A. S., Petrasso, R. D., and Švestka, Z.: 1979, *Solar Phys* **62**, 123.

Pick, M.: 1961, *Ann. Astrophys.* **24**, 183.

Schadee, A., De Jager, C., and Švestka, Z: 1983, *Solar Phys.* **89**, 287. (Abbreviated as SDJS).

Sheeley, N. R., Howard, R. A., Koomen, M. J., Michels, D. J., Schwenn, R., Muhlhauser, K. H., and Rosenbauer, H.: 1984, *J. Geophys. Res.* **90**, 163.

Sturrock, P. A.: 1968, *IAU Symp.* **35**, 471.

Švestka, Z.: 1984a, *Solar Phys.* **94**, 171.

Švestka, Z.: 1984b, *Mem. Soc. Astron. Ital.* **55**, 725.

Švestka, Z. and Poletto, G.: 1985, *Solar Phys.* **97**, 113.

Švestka, Z., Stewart, R. T., Hoyng, P., van Tend, W., Acton, L. W., Gabriel, A. H., Rapley, C. G., and 8 co-authors: 1982, *Solar Phys.* **75**, 305.

Švestka, Z, Schrijver, J., Somov, B., Dennis, B. R., Woodgate, B. E., Fürst, E., Hirth, W., Klein, L., and Raoult, A.: 1983, *Solar Phys.* **85**, 313.

Tsuneta, S., Takakura, T., Nitta, N., Ohki, K., and 4 co-authors: 1983, *Solar. Phys.* **86**, 313.

Wild, J. P.: 1969, *Solar Phys.* **9**, 260.

Wu, S. T., de Jager, C., Dennis, B. R., Hudson, H. S., Simnett, G. M., Strong, K. T., and 15 co-authors: 1985, in M. R. Kundu and B. E. Woodgate (eds.), *Proc. SMM Workshop on Solar Flares*, (in preparation).